

A SIMULATION STUDY OF A MOBILE ROBOT WITH SELF-LOCKING SPEED REDUCERS

Janusz Frączek, Marek Surowiec and Marek Wojtyra

Institute of Aeronautics and Applied Mechanics
Warsaw University of Technology, Nowowiejska 24, 00-665 Warsaw, Poland
e-mail: {jfraczek, msurowiec, mwojtyra}@meil.pw.edu.pl
web page: <http://www.meil.pw.edu.pl/iaam>

Keywords: Robot, Gear, Friction, Simulation.

Abstract. *The paper presents a simulation model of a mobile robot. The robot is equipped with four track systems wrapped around four movable and independently driven track holders, in which the driving torques are transmitted to the track systems via speed reducers. The study is focused on friction effects in gearing, and especially on the self-locking properties. A simplified mathematical model of friction in a speed reducer is presented. The model is based on the Coulomb friction law and on the analogy between a gear and a wedge mechanism. This friction model is implemented in general purpose simulation software in which the tracked mobile robot is modelled. A multibody model of the robot is briefly described. Simulation results obtained for different friction levels, varying from friction absence to friction beyond the self-locking limit, are compared and discussed. The robot motors are also modelled and requirements for electric power in various operating conditions are estimated.*

1 INTRODUCTION

Designing and assembling of a Small Mobile Robot (SMR) is one of the tasks of the project [1], which deals with integrated mobile system supporting anti-terrorist and anti-crisis actions. The concept of the SMR structure is depicted in Fig 1. This vehicle is planned to be an unmanned platform capable of carrying various sets of equipment (cameras, detectors, manipulator arm etc.) into potentially hostile and hardly accessible environment.

The design process is supported by multibody modelling and simulation of the SMR. The objectives of modelling are to study dynamic behaviour of the robot and to estimate power consumption as well as forces and torques acting on the robot (especially driving torques, required for typical manoeuvres). The virtual model presented in this article was built prior to the first hardware prototype.

The robot being designed is equipped with four track systems wrapped around four movable and independently driven track holders (Fig. 1). It is propelled by eight electric motors, and the driving torques are transmitted to the tracks and track holders via speed reducers. The transmitted power is partially dissipated due to friction occurring between cooperating elements of gears. The gears in the track holders power transmission systems are self-locking (i.e. irreversible), thus friction effects play extremely important role [2, 3].

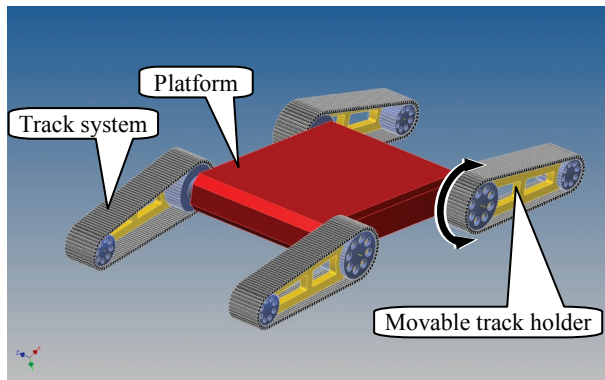


Figure 1: A Small Mobile Robot (CAD visualisation).

One of the most important objectives of the SMR simulation is to gain quantitative information on power consumption and torque requirements in the presence of friction, especially in the case of self-locking gears. Since a big portion of transmitted power is dissipated, irreversible speed reducers are characterized by relatively small efficiency. However, when motion is ceased and an external load applies a dynamic or static torque to the output gear shaft no input torque is required to keep the system in a state of rest [2, 3]. Thus, when motor is stopped no power is consumed (in case of reversible gears, a stopped motor must develop a non-zero torque to balance external loads).

This paper is focused on studying effects of friction forces occurring in the power transmission system. Reduction gears with different friction levels (ranging from frictionless to self-locking ones) are investigated and requirements for driving torques, as well as for electric power, are estimated. The movable track holders actuation and transmission systems are examined.

At the early stage of the SMR design process various types of speed reducers were considered to be installed in the prototype. Therefore it was decided to develop a model of friction effects in speed reducer which is both quite simple and versatile. The versatility is understood here as ability of applying the same model to simulation of different types of gears, e.g., worm, cylindrical, bevel, epicyclic, etc. It was assumed that the developed model of a speed

reducer with friction effects must allow for establishing appropriate relations between input and output torques, and – obviously – must hold the ratio between input and output angular velocities. Since the model is going to be just a part of a bigger model of the whole vehicle, it is not necessary to delve deeply into construction details of the investigated gearing, and thus building separate models for each type of gearing should be avoided. The mathematical model of friction in speed reducer presented in this paper is based on the Coulomb friction law and exploits the analogy between a reducer and a wedge mechanism.

In order to account for electric power consumption it was useful to utilise models of DC motors. A radically simplified model of robot control system was also built. The developed models of friction effects within gear train, as well as models of motors and controllers, were implemented in general purpose simulation software in which the SMR was modelled.

The simulation model of mobile robot actuation and transmission system can operate in two distinct modes. In the first case, driving constraints are imposed on each motor shaft rotation. Due to kinematic nature of motion definition, this mode of model operation is referred to as “kinematic”. In the second case, electro-mechanical properties of motors are taken into account, and driving constraints are replaced by driving torques. This mode of model operation is referred to as “dynamic”, and it allows not only for testing robot with motors but also for including some control system features.

Simulation results, obtained for different operation modes and different friction levels, are presented and discussed in the paper. Torque and power requirements during track holders configuration changes are investigated.

2 MATHEMATICAL MODELS OF ROBOT DRIVE SYSTEM COMPONENTS

2.1 Modelling of friction in speed reducers

It was assumed that friction between cooperating elements of a speed reducer is described by the Coulomb dry friction model. It was also assumed that masses of moving parts of the reducer are negligible (inertial properties of the reducer shafts can be accounted for by introducing appropriate amendments into inertial properties of vehicle parts connected to the shafts).

In a multibody simulation model an ideal, frictionless gear can be represented by appropriate constraints that enforce proper relations between input and output shaft motion. We decided to use this kind of model and to introduce additional torque responsible for friction effects. Thus, our considerations are focused on friction torque calculation.

The mathematical model of friction in a speed reducer is based on analogy between the reducer and a wedge mechanism. Note that two-sided wedge, depicted in Fig. 2, is introduced in order to allow the normal force to reverse its direction. The analogy between the wedge mechanism and a screw or worm gear is obvious. In case of other types of gears, the mathematical model based on wedge mechanism equations can be treated as coarse approximation.

In the simplified model of a speed reducer force \mathbf{F} corresponds to the driving torque which is applied to the input shaft I , and force \mathbf{P} corresponds to the external load torque which is applied to the output shaft O . It is assumed that friction forces are acting only in the kinematic pair formed by bodies I and O . Since available motor acceleration is limited and masses of gear elements are assumed to be negligibly small, the inertial forces are not taken into account.

The inclination angle α (Fig. 2) is related to the speed reducer gear ratio r (i.e., the ratio between input and output angular velocity) which can be expressed by the following equation:

$$\tan \alpha = 1/r. \quad (1)$$

Let us consider body I placed (without clearances) between two inclined planes belonging to body O , as shown in Fig. 2. The external force \mathbf{F} is applied to body I , and body O acts upon body I with normal force \mathbf{N} and friction (tangent) force \mathbf{T} . Vector \mathbf{v} represents the velocity of body I with respect to O . The external force \mathbf{P} is applied to body O , and body I acts upon body O with forces $-\mathbf{N}$ and $-\mathbf{T}$. The forces acting between the wedge mechanism casing (body C) and bodies I and O are perpendicular to respective axes of relative motion (and omitted in the figure). Figure 2 presents positive directions of the velocity and force vectors, i.e. if forces are directed as shown in the figure, the corresponding scalar values F , P , N and T are positive, otherwise they are negative (scalar value F , e.g., can be treated as a “signed” magnitude of vector \mathbf{F} , with the sign responsible for indicating the vector direction).

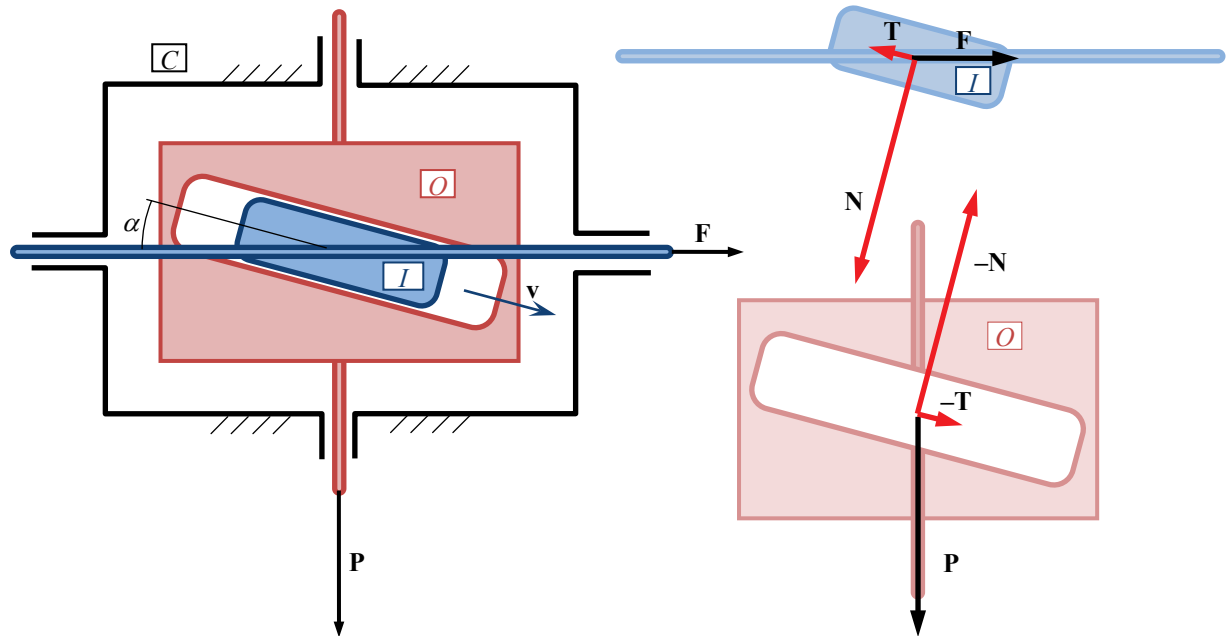


Figure 2: Distribution of forces in a wedge mechanism.

The following scalar equations of force equilibrium can be formulated for body I and O , respectively:

$$F = N \sin \alpha + T \cos \alpha, \quad (2)$$

$$P = N \cos \alpha - T \sin \alpha. \quad (3)$$

Equation (2) multiplied by $\sin \alpha$ and added to Eq. (3) multiplied by $\cos \alpha$, yields:

$$N = P \cos \alpha + F \sin \alpha. \quad (4)$$

Let us start discussing friction from less complicated case of kinetic friction, which occurs when the relative velocity \mathbf{v} is non-zero. In this case the relation between the normal load and the friction force can be expressed as:

$$T = \mu_K |N| \operatorname{sgn}(v), \quad (5)$$

where μ_K is the coefficient of kinetic friction.

The situation is more complicated when the relative velocity \mathbf{v} equals zero. This is the case of static friction. The maximum possible static friction force can be calculated as:

$$T_{\max} = \mu_s |N|, \quad (6)$$

where μ_s is the coefficient of static friction.

Equation (3) multiplied by $\sin\alpha$ and subtracted from Eq. (2) multiplied by $\cos\alpha$, yields the formula for tangent force:

$$T = F \cos \alpha - P \sin \alpha. \quad (7)$$

The external forces applied to the wedge mechanism are balanced by the static friction force, as long as the friction force is less than T_{\max} and greater than $-T_{\max}$. Otherwise, the external forces overcome the force of static friction and cause sliding to occur, thus the static friction transits into kinetic friction (at the moment of transition the relative velocity is zero, however, the relative acceleration is non-zero). Hence, the friction force at zero relative velocity can be calculated using the following expression:

$$T = \begin{cases} T_{\max} & \text{when } F \cos \alpha - P \sin \alpha \geq T_{\max} \\ -T_{\max} & \text{when } F \cos \alpha - P \sin \alpha \leq -T_{\max} \\ F \cos \alpha - P \sin \alpha & \text{otherwise} \end{cases}. \quad (8)$$

The considerations presented so far are valid for any values of friction coefficients, thus the equations can be utilised for both self-locking (irreversible) and back-driving (reversible) gears. Since the self-locking is a very important property of power transmission system, the conditions for self-locking of the considered wedge mechanism should be discussed.

The wedge mechanism is a self-locking one when the coefficient of friction is big enough. The dynamic self-locking occurs when for input force equal zero ($F = 0$), the magnitude of kinetic friction force (see Eq. (5)) is greater than the magnitude of tangent component of the external forces (see Eq. (7)). Two important cases should be considered. The first, when force \mathbf{P} is directed upwards (thus, in accordance to the discussed earlier sign convention, $P < 0$) and the body O is moving upwards as well (thus, $v > 0$). In the second case, the force is directed downwards ($P > 0$) and the body O is also moving downwards ($v < 0$).

In the first case, the condition for self-locking can be expressed as:

$$\mu_K |N| \operatorname{sgn}(v) > F \cos \alpha - P \sin \alpha. \quad (9)$$

Substituting $F = 0$ and Eq. (4) into Eq. (9) one obtains (for $P < 0, v > 0$):

$$-\mu_K P \cos \alpha > -P \sin \alpha, \quad (10)$$

and then (noticing that $-P > 0$):

$$\mu_K > \frac{\sin \alpha}{\cos \alpha} = \tan \alpha. \quad (11)$$

In the second case (note that this time friction force acts in opposite direction, thus inequality sign in Eq. (9) must be reversed), analogous considerations lead to exactly the same self-locking condition (11).

The static self locking occurs when for input force equal zero ($F = 0$), the magnitude of static friction force (see Eq. (8)) is greater than the magnitude of tangent component of the external forces. The condition for static self locking is similar to Eq. (11), this time, however,

the static friction coefficient is taken into account:

$$\mu_s > \tan \alpha . \quad (12)$$

In some manufactured gears a preload is introduced in order to diminish clearances and reduce backlash effects. When preload is present, force between gear elements is non-zero even when input and output torques are zero. To account for preload in our simplified model, it can be assumed that the body is compressed between wedge planes with force $N_0 > 0$. If the external force acting on the body is small, the contact between the body and the wedge planes is bilateral. The contact is unilateral when the magnitude of normal force $|N|$ (see Eq. (4)) is greater than N_0 . It means that the normal force between the body and the wedge planes is equal or greater than N_0 . Thus, to account for preload it is sufficient to replace Eq. (5) by the following expression:

$$T = \mu_k \operatorname{sgn}(v) \cdot \max(N_0, |N|), \quad (13)$$

and Eq. (6) by:

$$T_{\max} = \mu_s \cdot \max(N_0, |N|). \quad (14)$$

Concluding this section we can state that, in the case of kinetic friction, to calculate friction force one should use Eq. (4), and then Eq. (13). In the case of static friction, equations (4), (14) and (8) should be subsequently utilized.

2.2 Modelling of DC motors

Permanent magnet DC motors are used to actuate the mobile robot. Mechanical parts of the motors, i.e., stators and rotors are modelled in the multibody software (which automatically formulates and solves equations of motion), whereas equations describing electrodynamics of the motors must be derived and appended to the multibody model.

A simplified DC motor circuit diagram is presented in Fig. 3. Parameters R and L represent resistance and inductance of armature winding, respectively. U_e represents the back-emf (electromotive force) which is generated when the rotor revolves. Thus, the following equation of electric circuit can be formulated [4, 5]:

$$U(t) = U_e(t) + L \dot{I}(t) + R I(t), \quad (15)$$

where U is the voltage of power supply, I is the armature current and t denotes time.

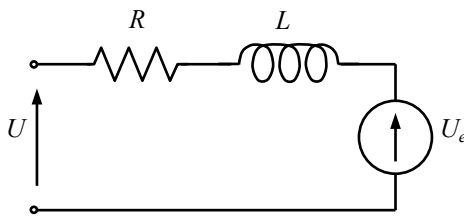


Figure 3: Simplified permanent magnet DC motor circuit diagram.

The back-emf U_e is proportional to the angular velocity ω of the motor and the torque M generated by the motor is proportional to the current through the windings, hence:

$$U_e(t) = K_e \cdot \omega(t), \quad M(t) = K_m \cdot I(t), \quad (16)$$

where K_e and K_m are the voltage and torque constants, respectively (note that $K_e \approx K_m$).

Equations (15) and (16) can be combined to obtain:

$$\dot{I} = (U - K_e \omega - RI)/L. \quad (17)$$

The above equation is integrated during direct dynamics calculations (for each motor). Then Eq. (16) is used to driving torque calculation. This torque, acting between the stator and the rotor, is transmitted via the speed reducer to the movable track holder.

Instantaneous electric power consumption can be calculated as:

$$P_E(t) = U(t) \cdot I(t). \quad (18)$$

In a special case of halted motor and constant motor load, Eq. (16) and Eq. (17) (for $\dot{I} = 0$ and $\omega = 0$) combined with Eq. (18) result in the following:

$$P_E = R \cdot I^2 = \frac{R}{K_m^2} \cdot M^2. \quad (19)$$

Thus, when the motor operates under stall conditions, the electric power is proportional to the square of generated torque.

Instantaneous mechanical power consumption can be calculated as:

$$P_M(t) = M(t) \cdot \omega(t). \quad (20)$$

Note that mechanical and electric power requirements can be quite different, especially when the motor develops torque at zero angular velocity.

2.3 Modelling of controllers

Output torque generated by an electric motor is a function of input voltage, armature current and rotor angular velocity [4, 5]. Robot control system collects information on the current state of the vehicle (supplied by sensors) and compares them with information on the desired state. The control process, resulting in supplying the motor with input voltage necessary for tracking the desired trajectory is usually quite complicated in a real robotic system [6]. In order to focus the study on friction effects in gearing, the model of motors and control system was significantly simplified.

It was assumed that the input voltage U is described by the following equation:

$$U = k_\varphi(\varphi - \varphi_D) + k_\omega(\omega - \omega_D), \quad (21)$$

where φ_D is the desired angle of track holder rotation (with respect to the robot basis), φ is the actual angle of rotation, ω_D and ω are the respective angular velocities, k_φ and k_ω are constant values. Note that Eq. (21) corresponds to PD control algorithm [7].

In the real control system the pulse-width modulation (PWM) technique is used [8], thus U given by Eq. (21) represents the effective rather than instantaneous voltage. The effective input voltage may vary between U_{\min} and U_{\max} , thus Eq. (21) must be amended to account for control signal saturation:

$$U = \begin{cases} U_{\max} & \text{for } k_\varphi(\varphi - \varphi_D) + k_\omega(\omega - \omega_D) \geq U_{\max} \\ U_{\min} & \text{for } k_\varphi(\varphi - \varphi_D) + k_\omega(\omega - \omega_D) \leq U_{\min} \\ k_\varphi(\varphi - \varphi_D) + k_\omega(\omega - \omega_D) & \text{otherwise} \end{cases}. \quad (22)$$

In case of irreversible speed reducers one more modification is introduced to the method of input voltage calculation. It is obvious that control error ($\varphi - \varphi_D$) is a small value but seldom

it is exactly equal zero. Thus, when the motor is stopped and static friction locks the reducer, the input voltage calculated using Eq. (22) is non-zero. Applying this voltage would result in generating torque too small to overcome friction forces, which is pointless (the control error would not decrease). That is why, in case of irreversible reducers, the method of input voltage calculation is modified: when the motor is stopped and simultaneously the desired angular velocity ω_D is zero, the input voltage, originally given by Eq. (22), gradually decreases its magnitude to zero. When the desired velocity becomes a non-zero value, Eq. (22) is again used in input voltage calculation. Similar procedure is applied in the case of speed reducers with friction below the self-locking limit: the magnitude of input voltage gradually decreases to the minimal value required to keep the reducer in the state of rest. This time, however, this minimal value is greater than zero.

3 MULTIBODY MODEL OF THE SMALL MOBILE ROBOT

3.1 Simulation model of a tracked vehicle

A commercial multibody simulation package [9] was used to build a model of the SMR (Fig. 5). The robot is treated as a system of bodies interconnected by kinematic pairs or contact elements. The modelled bodies are rigid, whereas flexibility effects are considered in auxiliary elements, like springs, bushings, etc. The simulation software allows for dynamic analysis of SMR. Equations of motion for multibody system are formulated automatically, however, equations describing gearing friction, as well as electric motors and controllers must be separately implemented in the software.

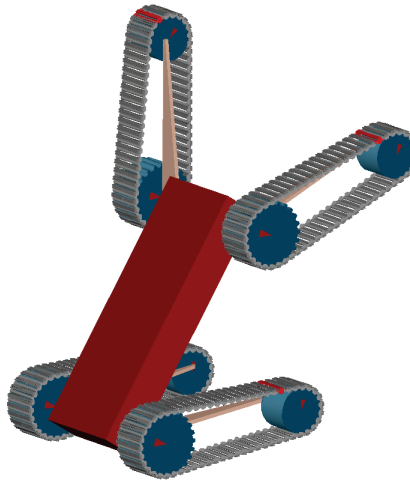


Figure 4: A multibody model of the SMR.

A typical multibody model consists of bodies, joints and applied forces. Usually, the kinematic structure of a multibody system does not change. However, when a tracked vehicle is considered, track segments frequently change their connectivity, and kinematic structure of the model changes almost continuously. Each track segment is connected with two neighbouring segments, and – depending on its current position – it can be separated from other bodies, or it can remain in contact with the terrain or with one of the suspension wheels, or with both – wheel and terrain at the same time. Consequently, to avoid kinematic structure changes in the multibody model, interactions between track segments and other bodies are introduced as contact forces rather than as kinematic constraints [10].

Our present study is not focused on track systems modelling, however – in general – modelling of track contact forces is crucial for simulation reliability and efficiency. The rigid body contact model [9] used during simulations is relatively simple, being a reasonable compromise between accuracy and effectiveness. In the vehicle model the number of bodies and contact forces is large, mainly due to large number of track segments, and thus the usage of more sophisticated and mathematically more complex model of contact phenomena would result in very long simulation time. The rigid body contact model is a reasonable compromise between simulations efficiency and accuracy.

The simulation software analyzes shapes and instantaneous positions of these parts for which contact was declared, detects contact occurrences and, at the points of contact, determines the penetration depth and velocity. The contact force can be decomposed into two components: normal and tangent to the surface of contact. The normal component is given by the following equation:

$$F = \begin{cases} \max(0, k \cdot x^e - c \cdot \dot{x}) & x > 0 \\ 0 & x \leq 0 \end{cases}, \quad (23)$$

where x denotes the penetration depth. Stiffness k and exponent e are constants specific to the modelled problem (e.g., they depend on terrain and track properties [11]). The damping coefficient c is a function of penetration depth:

$$c(x) = \begin{cases} 0 & x \leq 0 \\ c_{\max} \left(\frac{3}{h^2} x^2 - \frac{2}{h^3} x^3 \right) & 0 < x \leq h \\ c_{\max} & x > h \end{cases}, \quad (24)$$

where the distance h and maximum damping c_{\max} are constants specific to the modelled problem.

The tangent component of contact force is calculated using the Coulomb friction model.

There are no straight rules telling how to choose parameters of the contact model. If it is possible, the simulation results should be – first of all – confronted with experimental data. In our case satisfactory parameters were found after a number of test simulations; the obtained results were compared with data available for similar vehicles. The simulations also showed that the obtained results are not highly sensitive to changes of the values of contact parameters. Thus, even if the parameter estimation is not very accurate, the simulation results reliability is not endangered.

3.2 Simulation model of speed reducers

As it was explained earlier, the model is focused on establishing proper relations between input and output torque, as well as between input and output speed (and thus, the model reflects power flow and losses). Construction details of the simulated reducers (bearings, gear teeth, etc.) are neglected or modelled in a simplified way. The presented method of modelling can be applied to various types of speed reducers.

From the point of view of a software user, the reducer model consists of three bodies: the input and output shafts and the casing (Fig. 5), regardless the actual type and complexity of the investigated reducer. Masses and moments of inertia of the reducer bodies are negligibly small when compared with inertia of the other parts of simulated vehicle. Moreover, inertial properties of vehicle parts connected to the reducer can be modified to account for the reducer

parts inertia. Equations presented in section 2.1 are used to calculate friction torque. In the simulation model this torque is applied to the input shaft as an additional load.

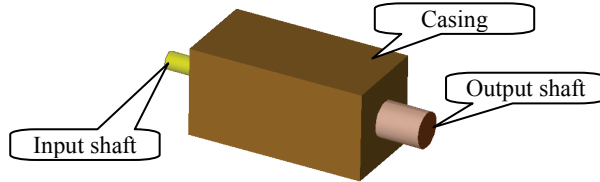


Figure 5: Simulation model of a speed reducer.

The simulation model is parameterized. The basic parameter is the gear ratio r . Parameter N_0 represents the modelled gear preload. Parameter μ is responsible for friction effects modelling; for the sake of simplicity, the same parameter is used for both static and kinetic friction. In the simplified mathematical model of a wedge mechanism μ is simply the coefficient of friction. In case of real gears modelling, this parameter may additionally depend on mechanism geometry. Any non-negative value of parameter μ is acceptable in the simulation model, thus it is possible to simulate a wide range of reducers, from frictionless to self-locking.

The simulation model can operate in “kinematic” or “dynamic” mode. In the “kinematic” mode driving constraints are imposed on angular position of DC motor rotor (which is connected to the speed reducer input shaft). Note that driving constraints are imposed on the input shaft, however, for the whole vehicle a dynamic (not kinematic) analysis is performed. In the “dynamic” mode a driving torque is applied to the rotor and then transmitted to the input shaft.

An important difference between two modes of model operation can be observed in the case of static friction occurring in the speed reducer. According to Eq. (8), the static friction torque balances the resultant of input and output torques. In the “dynamic” mode, the static friction torque can be uniquely determined, since the input torque is known. However, when driving constraints are imposed in the “kinematic” mode, the input torque cannot be uniquely determined, since the same motion (namely, the state of rest) can be obtained for various values of the input torque. Thus, in the “kinematic” mode, the static friction torque can have an arbitrary value between the minimum and maximum possible.

The simulation model of a reducer was built in such a way that in the case of static friction (when operating in the “kinematic” mode) among all the possible driving torques the one with the smallest magnitude is chosen. This additional condition is very important, since it makes the solution unique. Moreover, this condition is technically justified because the chosen input torque corresponds to the minimum electric power requirements.

It should be emphasized that from the physical point of view, the problem of finding the input torque, in case of a state of rest imposed by driving constraints, is not uniquely solvable. Solutions fairly different from those predicted by the simulation model are acceptable as well.

3.3 Simulation model of motors and controllers

The simulation software automatically generates only the equations describing mechanical properties of the model. Thus, the equations responsible for controllers and electrodynamics of motors were derived (see sections 2.2 and 2.3) and then included in the model (“dynamic” mode). At each numerical integration step input voltage and driving torque are calculated using Eq. (22) and Eq. (16), respectively. The armature current is governed by Eq. (17) which is integrated alongside with other differential equations for the whole multibody model.

4 SIMULATIONS

4.1 Objectives and variants of simulations

Robot motion along a horizontal plane was investigated during test simulations. The robot was changing configuration of its track holders when moving forward with constant velocity. The motion pattern was the same for both sides of the robot. The simulation study was focused on the friction effects in the track holders transmission systems. The input torques were transmitted to the movable track holders via speed reducers. Simulations for different levels of reducer friction, ranging from zero to above the self-locking limit ($\mu = \{0, 0.01, 0.02, 0.03\}$), were performed, whereas the gear ratio ($r = 50$) remained unchanged in all tests. During the first series of simulations the model was operating in the “kinematic” mode, and during the second series in the “dynamic” mode. Among other quantities, the input torques necessary to fulfil the robot motion requirements were calculated. Mechanical and electric power requirements were also computed.

Note that some parameter values used during simulations were chosen just to illustrate the discussed problems. These parameters do not reflect the actual properties of the designed SMR.

The analysed robot motion lasts ten seconds and can be divided into five phases. During the first phase (0-2 s) front and rear track holders are directed forward. Next (2-4 s), the rear track holders rotate backward. During the third phase (4-6 s) robot configuration remains unchanged. Then (6-8 s), all track holders rotate to move robot platform upwards, and finally, during the fifth phase of motion (8-10 s) the robot configuration is kept unaltered. The sequence of track holders configuration changes is presented in Fig. 6, and the assumed courses of the front and rear track holders angular positions with respect to the robot basis are presented in Fig. 7.

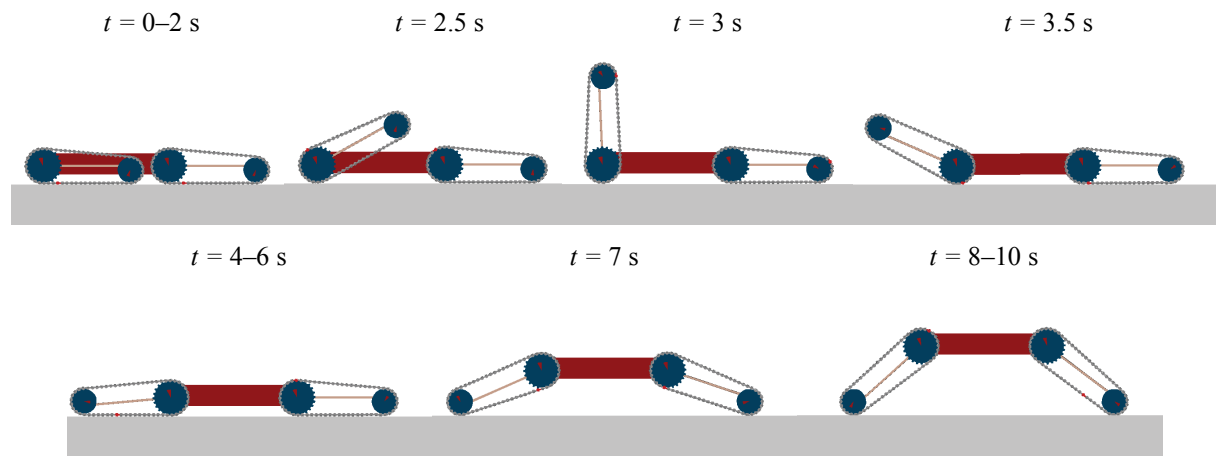


Figure 6: A sequence of track holders configuration changes.

It should be pointed out that in all “dynamic” mode simulations the same desired motion was required, however, in each case the gear friction level was different, thus controllers acted differently. Therefore, when robot motion is concerned, negligibly small differences between results obtained for subsequent simulations were observed.

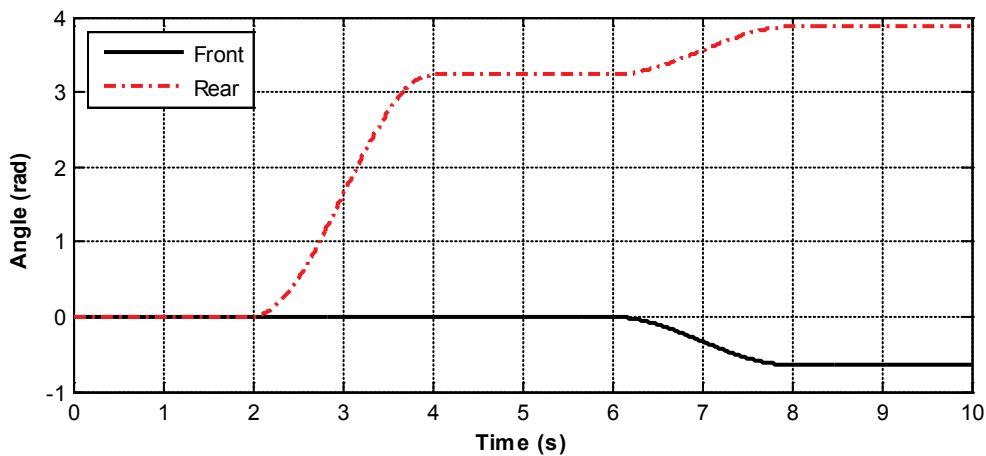


Figure 7: Desired angular positions of the front and rear track holders vs. time.

4.2 Motion as a result of imposing driving constraints

During the first series of tests driving constraints were imposed on the reducers input shafts motion (the required angular positions of track holders are presented in Fig. 7), and the resulting motion of the robot was calculated. Thus, the models of reducers were operating in the “kinematic” mode (recall that term „kinematic” concerns only the reducer input; for the whole system dynamic analyses were performed). The value of the friction coefficient was different in each simulation. The driving torques, calculated as reactions of driving constraints, were observed during simulations.

It should be pointed out that, in general, simulations in “kinematic” mode are intended be performed prior to selecting motors and to support the designer with data necessary to make this selection. Thus, the objective is to estimate requirements for driving torque and mechanical power during typical robot manoeuvres. The requirements for electric power cannot be established in “kinematic” mode. We decided to concentrate on demanded torque and not to discuss the requirements for mechanical power in this section; both mechanical and electric power requirements are presented and compared in the following section.

The first simulation was performed for frictionless reducers, thus the value of parameter μ was set to zero. Figure 8 presents the driving torque which must be applied to the input shaft of the rear track holder reducer to obtain the desired motion (see Fig. 7).

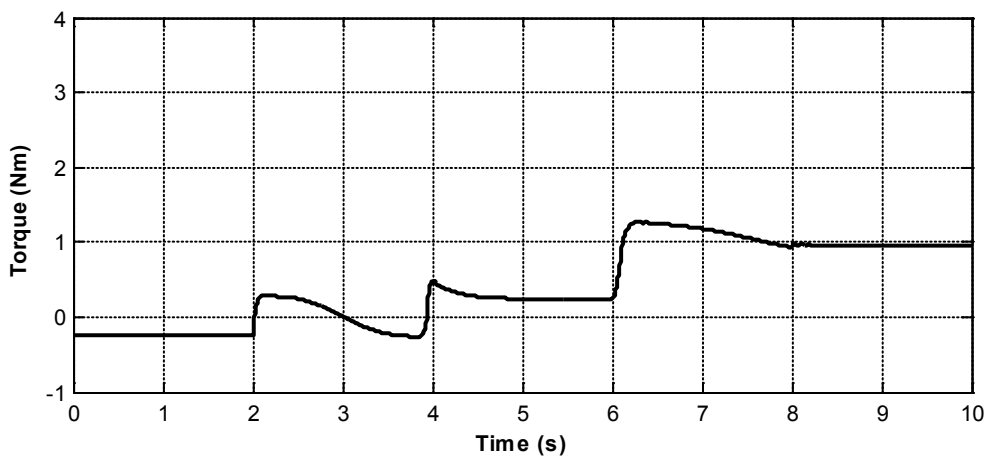


Figure 8: Input torque vs. time for a frictionless reducer.

As it could be expected, constant values of torque correspond to these phases of robot motion when track holders configuration remains unchanged, and non-constant values of torque are observed when the robot configuration varies. A few important details should be discussed.

Firstly, a rapid change in the input torque value is observed at $t = 2$ s, when the track holder starts to rotate. At this moment the area of track-ground contact decreases quickly and the centre of pressure moves swiftly backward to find its new position just under the track holder axis of rotation. Similar rapid changes of torque are observed around $t = 4$ s and $t = 6$ s when significant changes of centre of pressure position occur.

Secondly, when the track system is lifted and only the track segments under the driving wheel (the sprocket) are in contact with the ground, as it is observed for $t = 2\text{--}4$ s, the moment of ground forces about the track holder axis of rotation is close to zero. Hence, during this phase of motion, the external moment acting on the track holder results mainly from its own weight. That is why, as long as the track holder is moving upwards (2–3 s), the calculated torque is positive, whereas when the track holder is moving downwards (3–4 s), the torque is negative. It is worth noting that for $t = 3\text{--}4$ s the direction of input torque is opposite to the direction of rotation, thus the motor is serving as a brake (without the reverse torque, the track holder would accelerate due to gravity forces).

Thirdly, a non-zero torque is required to keep the track holder position unchanged. The observed torques are diverse for different robot configurations, since in each configuration distribution of mass as well as ground reaction forces is different.

Finally, it is observed that input torque is not constant just after $t = 4$ s despite the fact that track holders are not moving with respect to the base. To explain this phenomenon we shall recall that track-ground contact is modelled in terms of spring-damper forces (see Eq. (23)), thus after the configuration change the system needs some time to find a state of equilibrium. That is why torques exerted on track holders are non-constant for a while just after $t = 4$ s.

The rear track holder speed reducer output torque is presented in Fig. 9. In the case of a frictionless reducer, at every time instant, the output torque is simply $r = 50$ times larger than the input torque (compare Fig. 9 with Fig. 8). It should be emphasised that – for given robot motion – the reducer output torque should be always the same, regardless of the gear ratio and efficiency. Indeed, in our simulations the calculated output torques were almost identical for all tested levels of gear friction (and for both “kinematic” and “dynamic” modes of simulation), since differences in motion observed in subsequent simulations were negligible.

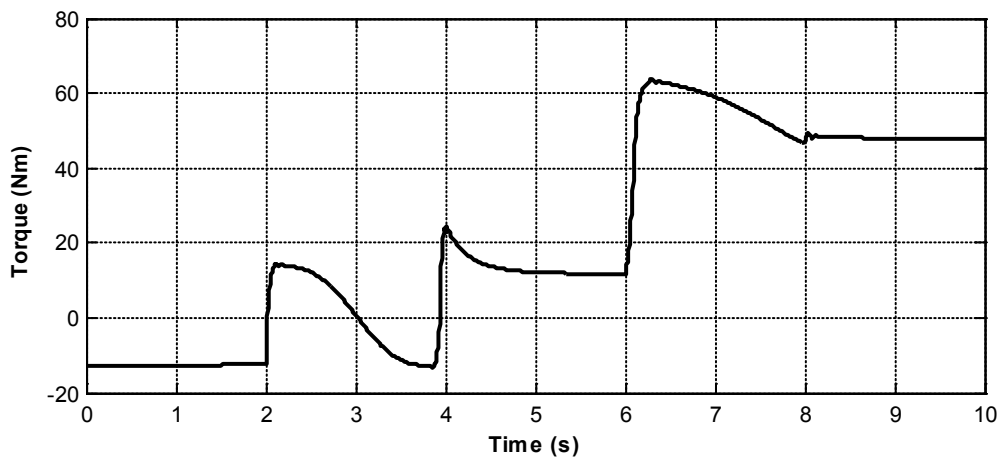


Figure 9: Output torque vs. time for the speed reducer of the rear track holder.

The second simulation was performed for the friction coefficient $\mu = 0.01$, thus the friction level was below the self-locking limit. The results are presented in Fig. 10, and qualitatively

they are similar to the results obtained for the case of a frictionless reducer. To analyse effects of friction in gearing, the quantitative differences between Fig. 10 and Fig. 8 should be discussed.

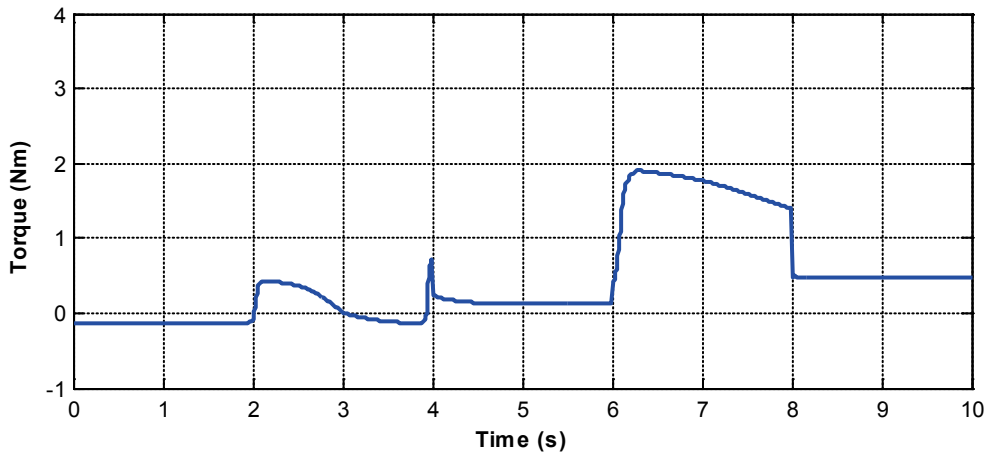


Figure 10: Input torque vs. time for a reducer with low friction.

It can be observed that in case of reducers with relatively low friction non-zero torque must be applied when the track holder is not rotating (0–2 s, 4–6 s, 8–10 s), however, magnitudes of required torques are much less than in case of a frictionless reducers. Situation is more complicated when the track holder is moving with respect to the base. When the motor lifts the track holder (2–3 s) or the whole robot (6–8 s) the demands for input torque are greater than in the frictionless case, since the motor must overcome friction forces. On the contrary, when the motor serves as a brake (3–4 s), the magnitude of required torque is less than in the frictionless case (when the track holder is moving downwards, the reducer friction forces are supporting the motor).

The third simulation was performed for the friction coefficient $\mu = 0.02$ which is exactly the self-locking limit, i.e. the reducer operational properties are placed at the border between self-locking and back-driving. The input torque calculated during this simulation is presented in Fig. 11. The results obtained now are significantly different from results gained in previous

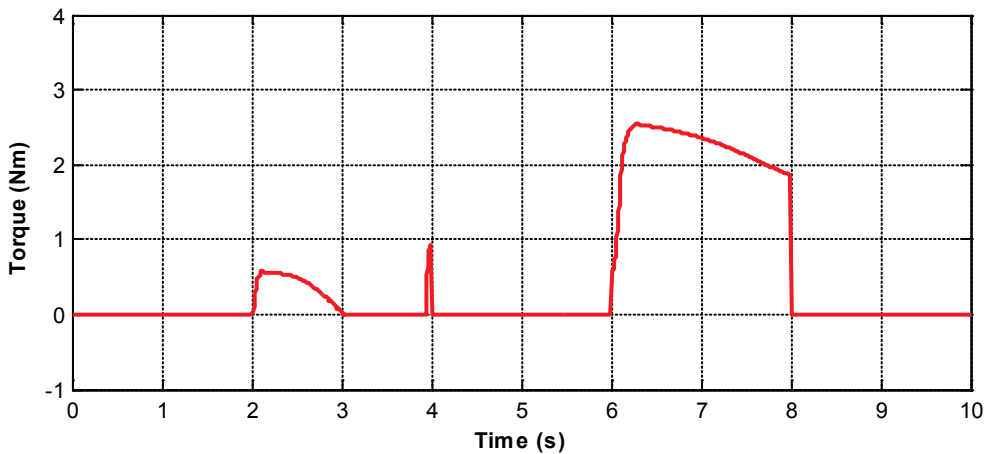


Figure 11: Input torque vs. time for a reducer with friction coefficient at the self-locking limit.

simulations. It is noticeable that the torque required to maintain constant position of the track holder is practically equal to zero. Moreover, the input torque required to decelerate the downwards moving track holder (i.e. when the motor is serving as a brake) is also very small.

On the other hand, torque required to lift the track holder (2–3 s) or the whole robot (6–8 s) is greater than in the previous cases. Similarly, the peak of torque observed around $t = 4$ s (when the rear track holder hits the ground) is greater than the earlier ones.

During the last simulation the modelled reducer was a self-locking one, with the friction coefficient $\mu = 0.03$. The calculated input torque is presented in Fig. 12. Three important issues should be pointed out in this case. Firstly, even when the track holder is moving downwards (3–4 s), it must be propelled. Unlike in other simulations, during this phase of motion the direction of driving torque and the direction of motor rotation are concordant. Secondly, when the track holder is stopped the required input torque is zero. It means that, since the gearing is irreversible, external loads applied to the stopped track holder are not transmitted back to the motors. Finally, the magnitude of torque required to lift the robot (6–8 s) is greater than in all previous cases. It should be reminded that in case of static friction (0–2 s, 4–6 s, 8–10 s) other input torque solutions are possible. As it was explained in section 3.2, the minimum-magnitude solutions were chosen.

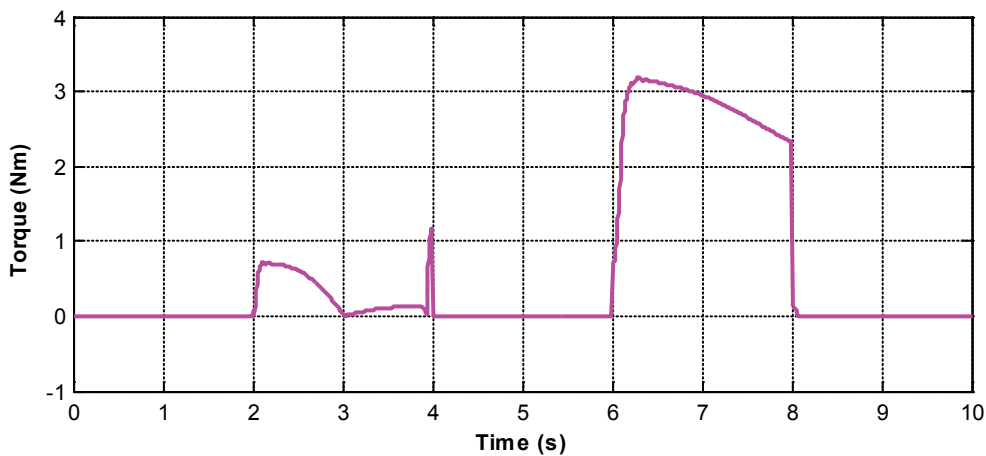


Figure 12: Input torque vs. time for a self-locking reducer.

The results of all four simulations are compared in Fig. 13. One should notice that taking into account friction forces in gearing is crucial for results credibility, especially when driving torques are solved for. Neglecting friction may result in calculating driving torque not only of a wrong magnitude but also of a wrong direction.

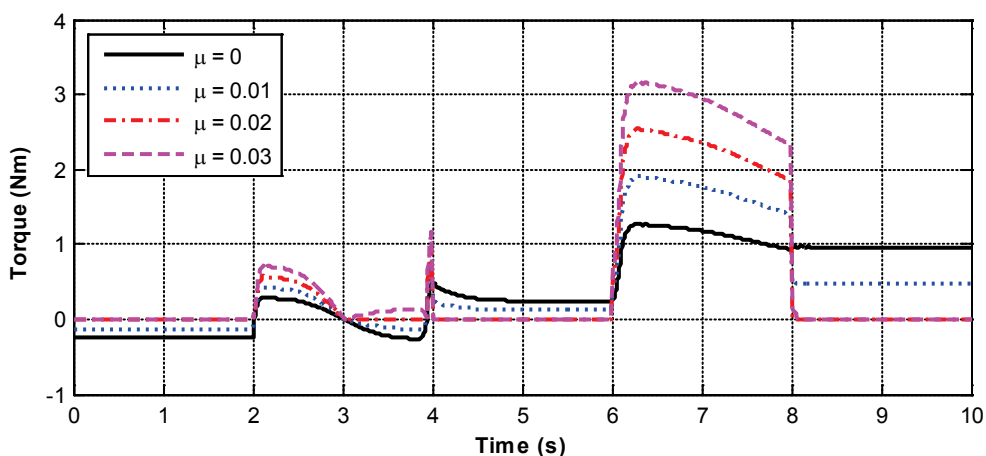


Figure 13: Input torques for different friction levels (“kinematic” mode).

4.3 Motion as a result of control and actuation

When simulation in “dynamic” mode is performed, equations describing motors and controllers (sections 2.2 and 2.3) are included in the model. In that case the speed reducer input torque results from control voltage, and not from driving constraints. Apart from driving torques, both mechanical and electric power requirements can be calculated.

Simulation tests similar to described in the previous section were performed. This time, however, the model was operating in the “dynamic” mode. Four simulations, for four different friction levels (the same as in the previous section), were carried out. The driving torques obtained from simulations are shown in Fig. 14.

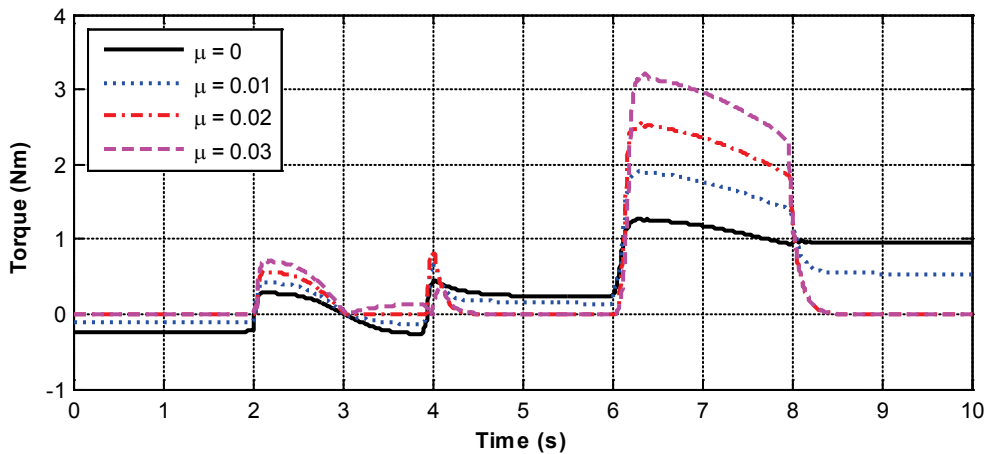


Figure 14: Input torques for different friction levels (“dynamic” mode).

The results presented in Fig. 14 (“dynamic” mode) are similar to the results showed in Fig. 13 (“kinematic” mode), and practically all comments presented in the previous section could be repeated here. The only important differences can be observed just after $t = 4$ s and $t = 8$ s. In the case of reducers with non-zero friction the torques decline to appropriate constant values gradually, and not immediately, as it was observed in the “kinematic” mode. This is the effect of decreasing the input voltage to the minimal required value (see section 2.3). Moreover, the peak of torque observed around $t = 4$ s is smaller, since – due to control process nature – the realised track holder trajectory is similar but not identical to the desired trajectory, and thus the changes of track-ground contact area go smoother.

The requirements for mechanical power (see Eq. (20)) for different friction levels are presented in Fig. 15. Obviously, when the track holder is not rotating, the mechanical power equals zero. As it should be expected, the demand for input power increases when friction level increases. The speed reducer output power was in each case the same, regardless of the gear friction. Note that in case of a frictionless reducer the input and output power are equal, thus the time course of output power can be read from Fig. 15.

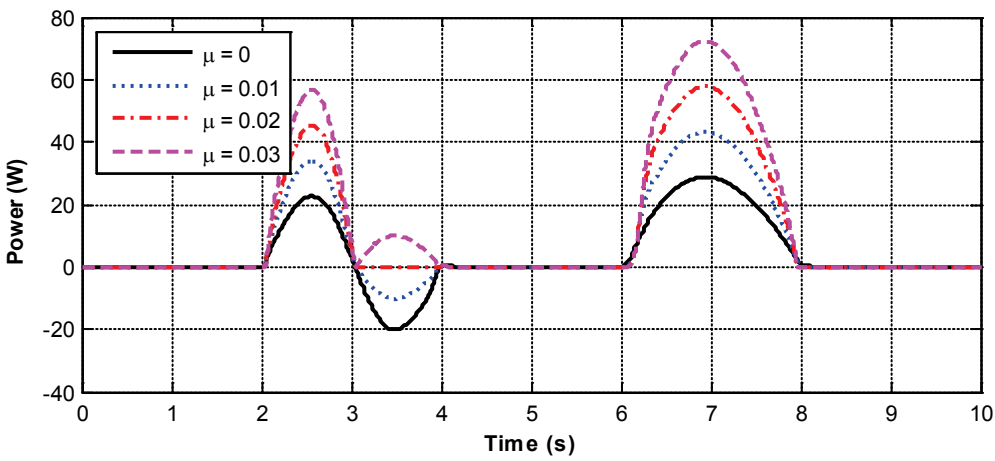


Figure 15: Mechanical power consumption for different friction levels.

Gear efficiency is usually defined as ratio of output power to input power. The concept of efficiency is useful when the direction of power transmission is constant and when motion without stops is concerned. In case of robotic applications, however, the idea of efficiency ratio is less useful. Note that proportions between input and output power are completely different, e.g., for $t=2\text{--}3$ s and $t=3\text{--}4$ s. That is why the speed reducer should be analysed in terms of direct comparison of input and output power rather than in terms of gear efficiency. The requirements for electric power (see Eq. (18)) for different friction levels are presented in Fig. 16. It is worth noting that – in the case of reducers with friction below self-locking level – even when the track holder is not rotating, the electric power is non-zero. As it should be expected, when the track holder is rotating, the demand for input power is higher at higher friction levels.

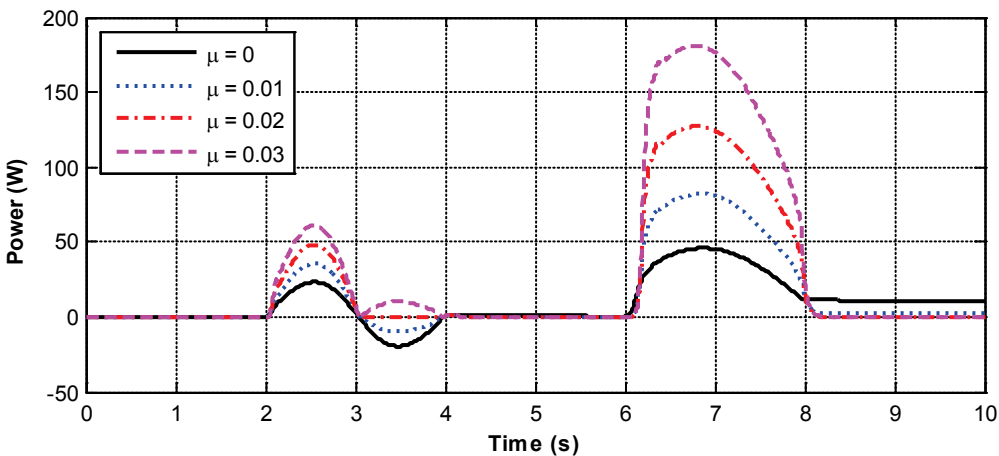


Figure 16: Electric power consumption for different friction levels.

It should be noted that efficiency of robot drive system depends not only on gear friction, since electric motor operating conditions are also very important. Figure 17 presents comparison of mechanical and electric power requirements for a frictionless speed reducer. Different types of relations between power demands can be distinguished. When the motor rotates at a high angular velocity and develops a small driving torque (2–4 s), the electric power is close to the mechanical power. On the contrary, when the angular velocity is low and the developed torque is high (6–8 s), the electric power consumption is much greater than the mechanical output power. Finally, when the motor produces a stall torque (0–2, 4–6, 8–10 s), the me-

chanical power is zero, whereas the electric power is non-zero. Obviously, the demands for electric power are higher for higher torque requirements (see Eq. (19)). The discussed results show that – for a frictionless reducer and different operation conditions – the efficiency of an electric drive system can vary from 0 to almost 1.

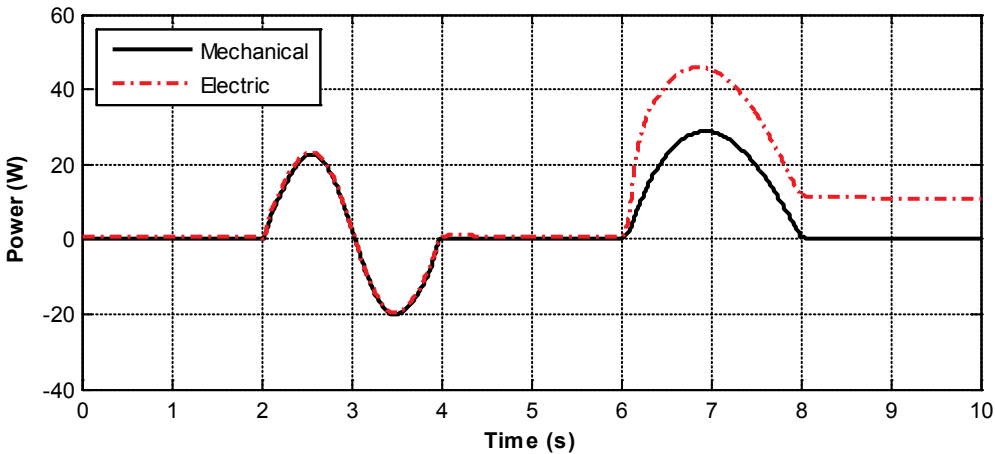


Figure 17: Mechanical and electric power requirements for a frictionless speed reducer.

5 CONCLUSIONS

A simple model of friction effects in reduction gears is presented in the paper. It may be used to account for friction in various types of reducers. The torques required to drive the system may be estimated prior to building the hardware prototype, and even prior to selection of gear type. The presented model of a reducer can work in two modes of simulation. In the “kinematic” mode vehicle motion is a result of imposing driving constraint. In the “dynamic” mode electro-mechanical properties of motors are taken into account, and motion results from supplying the required input voltage. Essential differences between these two modes were discussed.

A virtual model of the Small Mobile Robot was tested, the study was focused on the movable track holders actuation system. The performed tests show that accounting for gear friction is crucial for proper estimation of torque requirements. It is also shown that in case of using self-locking (irreversible) gears the calculated driving torques are completely different from the torques calculated for frictionless power transmission. Requirements for mechanical and electric power were calculated alongside with demands for driving torque.

The results of simulations show that – in case of the movable track holders – it is desirable to apply a speed reducers with friction level slightly above the self-locking limit. During the SMR operation the track holders are not going to rotate very often, thus it is crucial to keep them blocked without any power consumption. That is why speed reducers should be irreversible. On the other hand, when the track holders rotate, the power requirements are higher for higher friction levels, thus there is no point in pushing friction far beyond the self-locking limit.

The presented model supports the robot designer with quantitative results. Other typical robot manoeuvres, fairly different from the presented ones, can be studied using the same multibody model. An experimental verification of the simulated results is planned in the near future.

ACKNOWLEDGEMENTS

The project was co-financed by the European Regional Development Fund within the framework of the 1. priority axis of the Innovative Economy Operational Programme, 2007-2013, through grant PO IG 01.02.01-00-014/08-00, and by the Institute of Aeronautics and Applied Mechanics statutory funds.

REFERENCES

- [1] <http://www.projektproteus.pl/en/index.php>
- [2] A. A. Olędzki. Modeling and simulation of self-locking drives. *Mechanism and Machine Theory*, **6**, 929–942, 1995.
- [3] M. Leonesio, G. Bianchi, Self-locking analysis in closed kinematic chains. *Mechanism and Machine Theory*, **44**, 2038–2052, 2009
- [4] A. Hughes. *Electric motors and drives: fundamentals, types and applications*. Newnes, 2005.
- [5] P. C. Krause. *Analysis of Electric Machinery*. McGraw-Hill, 1986.
- [6] B. Siciliano, L. Sciavicco, L. Villani, G. Oriolo. *Robotics: Modelling, Planning and Control*. Springer, 2008.
- [7] K. Ogata. *Modern Control Engineering*. Prentice Hall, 2009.
- [8] D. G. Holmes, T. A. Lipo. *Pulse Width Modulation for Power Converters: Principles and Practice*. Wiley-IEEE Press, 2003.
- [9] MSC.ADAMS + ATV_2008r1. Documentation and help.
- [10] J. Slättengren. Utilization of ADAMS to Predict Tracked Vehicle Performance. SAE 2000 World Congress, Detroit, MI, USA, March, 2000.
- [11] J. Y. Wong. *Theory of Ground Vehicles*. John Wiley and Sons, 2008.